PROCEEDINGS OF SCIENCE

Baryon interactions from lattice QCD with physical masses —$S=-3$ sector: $\Xi\Sigma$ and $\Xi\Lambda-\Xi\Sigma$—

Noriyoshi Ishii[*,ab], **Sinya Aoki**,[bcd] **Takumi Doi**,[b] **Shinya Gongyo**,[be] **Tetsuo Hatsuda**,[bf] **Yoichi Ikeda**,[ab] **Takashi Inoue**,[bg] **Takumi Iritani**,[b] **Takaya Miyamoto**,[bc] **Keiko Murano**,[ab] **Hidekatsu Nemura**,[bd] **and Kenji Sasaki**[bc]

[a] *Research Center for Nuclear Physics, Osaka university, Osaka 567-0047, Japan*
[b] *Theoretical Research Division, Nishina Center, RIKEN, Wako 351-0198, Japan*
[c] *Yukawa Institute for Theoretical Physics, Kyoto University, Kyoto 606-8502, Japan*
[d] *Center for Computational Sciences, University of Tsukuba, Ibaraki 305-8571, Japan*
[e] *CNRS, Laboratoire de Mathématiques et Physique Théorique, Université de Tours, 37200 France*
[f] *iTHEMS Program and iTHES Research Group, RIKEN, Wako 351-0198, Japan*
[g] *Nihon University, College of Bioresource Sciences, Kanagawa 252-0880, Japan*
E-mail: ishiin@rcnp.osaka-u.ac.jp

We present lattice QCD results of baryon-baryon potentials in $S=-3$ sector, i.e., $\Xi\Sigma$ ($I=3/2$) potentials and $\Xi\Lambda$-$\Xi\Sigma$ coupled channel potentials ($I=1/2$) by using the 2+1 flavor gauge configurations with almost the physical quark masses generated on 96^4 lattice with $a^{-1}\simeq 2.3$ GeV and $L=96a\simeq 8.1$ fm where $m_\pi\simeq 146$ MeV and $m_K\simeq 525$ MeV. These potentials are obtained based on the time-dependent HAL QCD method with a non-relativistic approximation. Qualitative behaviors of the results are found to be consistent with those in the flavor SU(3) limit.

34th annual International Symposium on Lattice Field Theory
24-30 July 2016
University of Southampton, UK

*Speaker.

PoS(LATTICE2016)127

1. Introduction

One of the most important missions of J-PARC in the nuclear physics is experimental determination of hyperon-nucleon (YN) and hyperon-hyperon (YY) potentials. These potentials play an important role in studying the structures of the hyper-nuclei and properties of the neutron stars. Because of the short life time of the hyperons, it is not easy to determine the hyperon potentials for large $|S|$ sectors even by J-PARC, so that they focus mainly on $S=-1$ and -2 sectors. On the other hand, lattice QCD determination of hyperon potentials was recently proposed by HAL QCD collaboration, where Nambu-Bethe-Salpeter (NBS) wave functions are used to define the hyperon potentials which are faithful to the scattering data [1, 2, 3, 4]. Since the statistical noise reduces as the number of strange quarks increases, lattice QCD determination becomes easier for larger $|S|$.

Here, we present our results of hyperon-hyperon (YY) potentials for $S=-3$ sectors. We use 2+1 flavor lattice QCD gauge configurations generated by employing almost the physical pion mass $m_\pi \simeq 146$ MeV by using K computer at AICS [5].

2. Lattice QCD setup

We use the 2+1 flavor gauge configurations at almost the physical point generated by K computer at AICS [5]. They are generated on 96^4 lattice by employing the RG improved (Iwasaki) gauge action at $\beta = 1.82$ with the nonperturbatively $O(a)$-improved Wilson quark (clover) action at $(\kappa_{\rm ud}, \kappa_{\rm s}) = (0.126117, 0.124790)$ with $c_{\rm SW} = 1.11$ and the 6-APE stout smeared links with the smearing parameter $\rho = 0.1$. It leads to the lattice spacing $a^{-1} \simeq 2.3$ GeV ($a \simeq 0.085$ fm), the spatial extension $L = 96a \simeq 8.1$ fm, $m_\pi \simeq 146$ MeV, and $m_K \simeq 525$ MeV. In our calculation, 200 gauge configurations are used for the measurements. Quark propagators are generated by imposing the periodic boundary condition along the spatial direction while the Dirichlet boundary condition is imposed on the temporal direction on the time slice $t = t_1$ which is separated from the wall source as $t_1 - t_0 = 48$. 48 source points are used. Forward and backward propagations are combined by using the charge conjugation and time reversal symmetries to double the statistical data of two-point and four-point hyperon correlators. Each gauge configuration is used 4 times by using the hypercubic SO(4,$\mathbb{Z}$) symmetry of 96^4 lattice. Statistical data are averaged in the bin of the size 10, which is equivalent to 100 HMC trajectories. Jackknife prescription is used to estimate the statistical errors.

3. Single baryon sector

Effective mass plots for Λ, Σ and Ξ are shown in Fig. 1 for the two-point correlators with wall-sink and wall-source(wall-wall) together with the ones with point-sink and wall-source(point-wall). We perform single exponential fits simultaneously for the wall-wall and point-wall correlators with

$$C_{\rm WW}(t) \simeq a_{\rm WW} \exp(-mt), \quad C_{\rm PW}(t) \simeq a_{\rm PW} \exp(-mt), \tag{3.1}$$

by using three fit parameters, i.e., a baryon mass m, two overlaps parameters $a_{\rm WW}$ for the wall-wall correlator and $a_{\rm PW}$ for the point-wall correlators. The overlap parameters are used to determine the Z factors of local composite hyperon operators appearing in the limit $\psi(x) \to Z^{1/2}\psi_{\rm out}(x)$ as $x_0 \to +\infty$ where $\psi(x)$ and $\psi_{\rm out}(x)$ denote local composite operators and asymptotic fields for Λ,

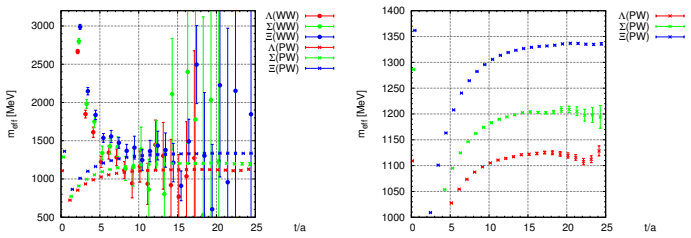

Figure 1: The effective mass plots of two-point correlators of Λ, Σ and Ξ for (WW) wall-wall and (PW) point-wall (lhs), and those for point-wall correlators (rhs).

Σ and Ξ. Note that, to obtain the $\Xi\Lambda$-$\Xi\Sigma$ coupled channel potentials, we need Z factors for Λ and Σ in the combination $\sqrt{Z_\Lambda/Z_\Sigma}$. For point-wall correlators, the plateau regions are identified as $15-20$ for Λ and Σ, and $20-25$ for Ξ. Since wall-wall correlators are too noisy to determine the plateau regions, we employ two regions (i) 10-15 and (ii) 15-20. Since the results do not change so much, i.e., the fit with 10-15 leads to $\sqrt{Z_\Lambda/Z_\Sigma}=1.02(3)$ whereas the one with 15-20 leads to $\sqrt{Z_\Lambda/Z_\Sigma}=1.05(9)$, we adopt the result with 10-15. The results of the hyperon masses are as follows: $m_\Lambda=1.121(3)$ GeV, $m_\Sigma=1.204(3)$ GeV and $m_\Xi=1.336(1)$ GeV.

4. $\Xi\Sigma$ single channel for $I=3/2$ sector

To obtain the $\Xi\Sigma$ potentials ($I=3/2$), we use the time-dependent HAL QCD method [6]. For this purpose, we define the R-correlator for $\Xi\Sigma$ as

$$R_{\Xi\Sigma}(\vec{x}-\vec{y},t)\equiv e^{+(m_\Xi+m_\Sigma)t}\,\langle 0|T\left[\Xi(\vec{x},t)\Sigma(\vec{y},t)\cdot\mathscr{J}_{\Xi\Sigma}(t=0)\right]|0\rangle\,, \tag{4.1}$$

where $\mathscr{J}_{\Xi\Sigma}$ denotes a wall source for $\Xi\Sigma$. R-correlator satisfies the time-dependent Schrödinger-like equation, which involves a fourth order time derivative [7]. The $\Xi\Sigma$ potential for $I=3/2$ should be obtained from this equation. However, since the numerical evaluation of the fourth order time derivative is not stable yet, we solve its non-relativistic approximation keeping the leading order of the derivative expansion of the non-local potential as

$$\left(-\frac{\partial}{\partial t}+\frac{\nabla^2}{2\mu}\right)R_{\Xi\Sigma}(\vec{r},t)=V_{\Xi\Sigma}(\vec{r})R_{\Xi\Sigma}(\vec{r},t), \tag{4.2}$$

where $\mu\equiv 1/(1/m_\Xi+1/m_\Sigma)$ denotes the reduced mass.

Fig. 2(a) shows the central potential of $\Xi\Sigma(I=3/2)$ for spin-singlet sector obtained in the region $t=10-15$. Since t-dependence is seen to be quite mild, we regard that rough convergence is achieved. We see that there is a repulsive core at short distance, which is surrounded by an attraction. Qualitative behavior is similar to NN case, which is because they belong to the same irreducible representation (irrep.) **27** in the flavor SU(3) limit. Fig. 2(b) and (c) show the central and the tensor potentials of $\Xi\Sigma(I=3/2)$ for spin-triplet sector obtained in the region $t=10-15$. Again, from the mild t-dependence, we regard that rough convergence is achieved. We see that qualitative behaviors are similar to NN potentials, i.e., the central potential has a repulsive core, which is surrounded by an attraction. This is because spin-triplet channel of $\Xi\Sigma(I=3/2)$ belongs to the irrep. $\mathbf{10}^*$ in the flavor SU(3) limit, to which spin-triplet sector of NN belongs.

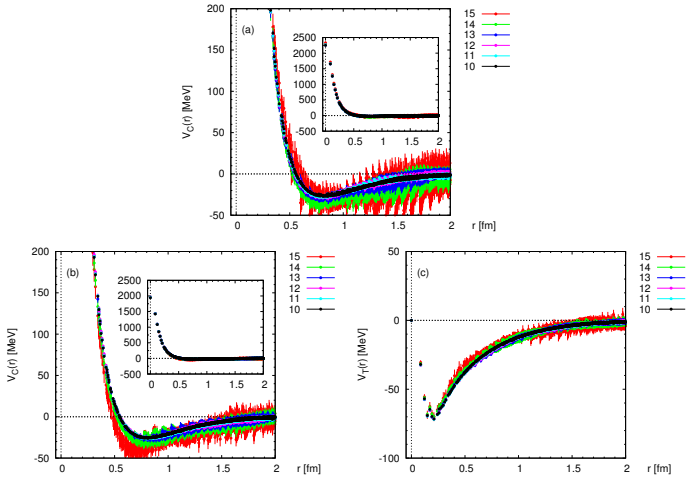

Figure 2: $\Xi\Sigma(I=3/2)$ potentials. (a) the central potential for spin-singlet sector, (b) the central potential for spin-triplet sector, (c) the tensor potential for spin-triplet sector.

In obtaining the $\Xi\Sigma$ potential, we replace the factor $e^{(m_\Xi+m_\Sigma)t}$ in Eq. (4.1) by a product of two-point correlators(point-wall) of Ξ and Σ so that the correlated statistical noises may cancel. Therefore, although the t-dependence of the potential is mild, t should be large enough to achieve the ground state saturation of two-point correlators of Ξ and Σ, i.e., $t \gtrsim 20$.

We use these potentials in the Schrödinger equation to obtain the scattering phase shifts. We first perform a fit to obtain smooth potentials, which are used to solve the Schrödinger equation. Fig. 3 shows the scattering phase shift obtained from the potentials in the region $t = 10-13$. We

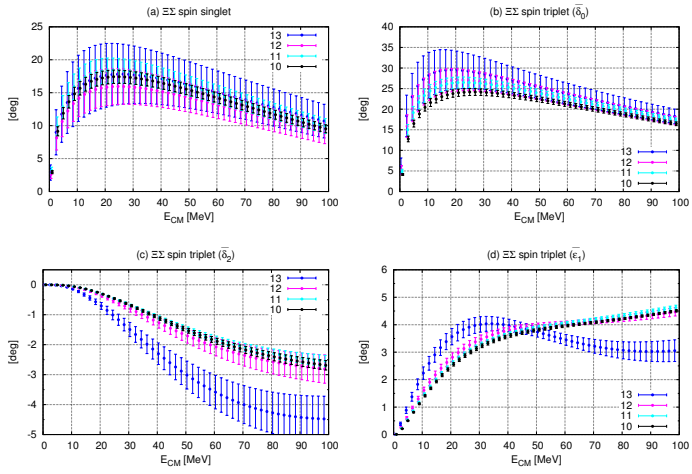

Figure 3: The scattering phase shift from $\Xi\Sigma(I=3/2)$ potentials given in Fig. 2 in the region $t=10-13$. (a) ${}^1S_0$ phase shift, (b) ${}^3S_1$ phase shift $\bar{\delta}_0$, (c) ${}^3D_1$ phase shift $\bar{\delta}_2$, (d) mixing parameter $\bar{\varepsilon}_1$.

see that qualitative behaviors are similar to the NN phase shift except for the two points (i) the strength is weak, and (ii) there is no bound state in spin-triplet sector.

The phase shift $\bar{\delta}_2$ and the mixing parameter $\bar{\varepsilon}_1$ at $t=13$ deviate from the others. This is

because of a technical reason that the fit of the potential falls into a slightly different minimum. Improvement of the statistics will resolve it.

5. $\Xi\Lambda$-$\Xi\Sigma$ coupled channel for $I=1/2$ sector

To obtain the $\Xi\Lambda$-$\Xi\Sigma$ coupled channel potential ($I=1/2$), we use coupled channel extension of time-dependent Schrödinger-like equation. We define the R-correlators

$$R_{\Xi\Lambda}(\vec{x}-\vec{y},t;\mathscr{J}) \equiv e^{+(m_\Xi+m_\Lambda)t}\langle 0|T\left[\Xi(\vec{x},t)\Lambda(\vec{y},t)\cdot\mathscr{J}(t=0)\right]|0\rangle \tag{5.1}$$

$$R_{\Xi\Sigma}(\vec{x}-\vec{y},t;\mathscr{J}) \equiv e^{+(m_\Xi+m_\Sigma)t}\langle 0|T\left[\Xi(\vec{x},t)\Sigma(\vec{y},t)\cdot\mathscr{J}(t=0)\right]|0\rangle, \tag{5.2}$$

where $\mathscr{J}=\mathscr{J}_{\Xi\Lambda},\mathscr{J}_{\Xi\Sigma}$ denote the wall sources for $\Xi\Lambda$ and $\Xi\Sigma$, respectively. The coupled channel extension of the time-dependent Schrödinger-like equation involves fourth time derivative [7]. Since the numerical evaluation of fourth time derivative is still unstable, we solve its non-relativistic approximation keeping only the leading order of the derivative expansion of the non-local potentials as

$$\begin{bmatrix}\left(-\frac{\partial}{\partial t}+\frac{\nabla^2}{2\mu_{\Xi\Lambda}}\right)R_{\Xi\Lambda}(\vec{r},t;\mathscr{J})\\ \left(-\frac{\partial}{\partial t}+\frac{\nabla^2}{2\mu_{\Xi\Sigma}}\right)R_{\Xi\Sigma}(\vec{r},t;\mathscr{J})\end{bmatrix} = \begin{bmatrix}V_{\Xi\Lambda;\Xi\Lambda}(\vec{r}) & \zeta_0\zeta^{+t/a}V_{\Xi\Lambda;\Xi\Sigma}(\vec{r})\\ \zeta_0^{-1}\zeta^{-t/a}V_{\Xi\Sigma;\Xi\Lambda}(\vec{r}) & V_{\Xi\Sigma;\Xi\Sigma}(\vec{r})\end{bmatrix}\cdot\begin{bmatrix}R_{\Xi\Lambda}(\vec{r},t;\mathscr{J})\\ R_{\Xi\Sigma}(\vec{r},t;\mathscr{J})\end{bmatrix}, \tag{5.3}$$

where $\zeta\equiv e^{(m_\Sigma-m_\Lambda)a}$ and $\zeta_0\equiv\sqrt{Z_\Lambda/Z_\Sigma}$ with Z_Λ and Z_Σ being the Z factors for the local composite operators of Λ and Σ, respectively. $\mu_{\Xi\Lambda}\equiv\frac{1}{1/m_\Xi+1/m_\Lambda}$ and $\mu_{\Xi\Sigma}\equiv\frac{1}{1/m_\Xi+1/m_\Sigma}$ denote the reduced masses for $\Xi\Lambda$ and $\Xi\Sigma$, respectively. Note that four unknowns $V_{\Xi\Lambda;\Xi\Lambda}(\vec{r})$, $V_{\Xi\Lambda;\Xi\Sigma}(\vec{r})$, $V_{\Xi\Sigma;\Xi\Lambda}(\vec{r})$ and $V_{\Xi\Sigma;\Xi\Sigma}(\vec{r})$ are determined from four equations in Eq. (5.3) with $\mathscr{J}=\mathscr{J}_{\Xi\Lambda}$ and $\mathscr{J}_{\Xi\Sigma}$.

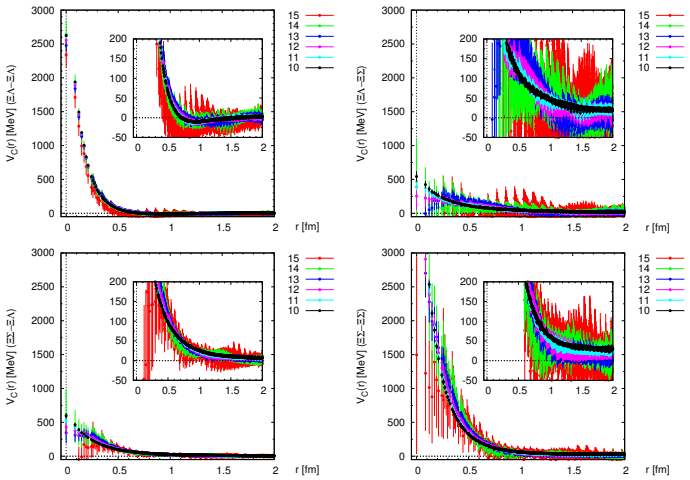

Figure 4: The $\Xi\Lambda$-$\Xi\Sigma$ ($I=1/2$) coupled channel central potentials in singlet spin channel.

Fig. 4 shows the $\Xi\Lambda$-$\Xi\Sigma$ coupled channel central potentials for spin-singlet sector obtained in the region $t=10-15$. We see that they are noisy, which is often the case if it contains the irrep. $\mathbf{8}_S$ in the flavor SU(3) limit. t-dependence is seen to be mild except that the long distance part of $\Xi\Lambda$-$\Xi\Sigma$ and $\Xi\Sigma$-$\Xi\Sigma$ potentials are still changing. Flavor SU(3) limit is helpful to understand

the qualitative behaviors of these potentials [8]. In the flavor SU(3) limit, these coupled channel potentials are related to those for the irreps. **27** and $\mathbf{8}_{\rm S}$ as $V_{\Xi\Lambda;\Xi\Lambda} = \frac{9}{10}V^{\mathbf{27}} + \frac{1}{10}V^{\mathbf{8}_{\rm S}}$, $V_{\Xi\Lambda;\Xi\Sigma} = V_{\Xi\Sigma;\Xi\Lambda} = -\frac{3}{10}V^{\mathbf{27}} + \frac{3}{10}V^{\mathbf{8}_{\rm S}}$ and $V_{\Xi\Sigma;\Xi\Sigma} = \frac{1}{10}V^{\mathbf{27}} + \frac{9}{10}V^{\mathbf{8}_{\rm S}}$. These relations together with the potentials for the irreps. **27** and $\mathbf{8}_{\rm S}$ given in Ref[8] qualitatively explain (i) the existence of attractive pocket at medium distance in $\Xi\Lambda$-$\Xi\Lambda$ potential, and (ii) strength of the repulsive cores of these four coupled channel potentials at short distance.

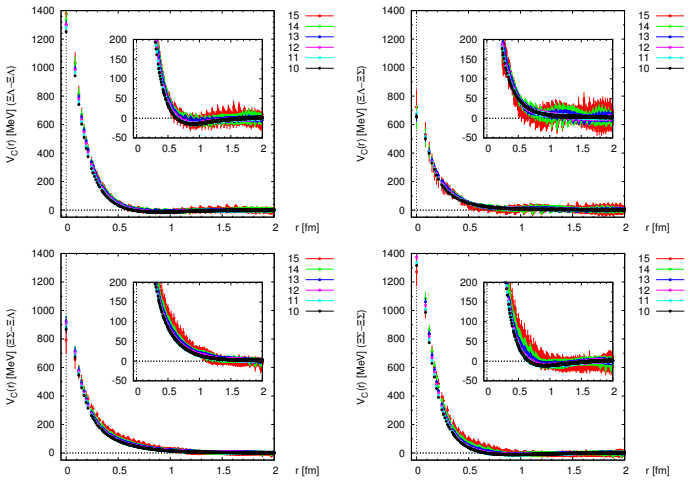

Figure 5: The $\Xi\Lambda$-$\Xi\Sigma$ ($I=1/2$) coupled channel central potentials in triplet spin channel.

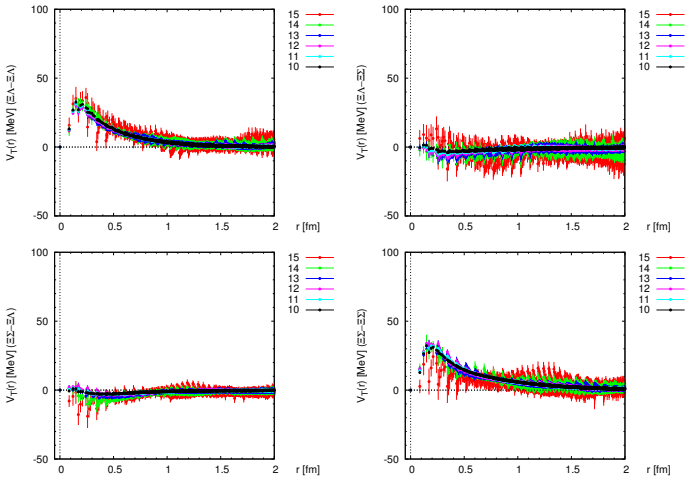

Figure 6: The $\Xi\Lambda$-$\Xi\Sigma$ ($I=1/2$) coupled channel tensor potentials in triplet spin channel.

Fig. 5 and Fig. 6 show the $\Xi\Lambda$-$\Xi\Sigma$ coupled channel central and tensor potentials, respectively, for spin-triplet sector obtained in the region $t = 10-15$. t-dependences are seen to be mild. But the central potentials for the $\Xi\Lambda$-$\Xi\Sigma$ and $\Xi\Sigma$-$\Xi\Lambda$ fail to achieve the complete convergence at long distance. To understand their behaviors qualitatively, the potentials in the flavor SU(3) limit are helpful again. In the flavor SU(3) limit, these coupled channel central and tensor potentials are related to those of the irreps. **10** and $\mathbf{8}_{\rm A}$ as $V_{\Xi\Lambda;\Xi\Lambda} = V_{\Xi\Sigma;\Xi\Sigma} = \frac{1}{2}V^{\mathbf{10}} + \frac{1}{2}V^{\mathbf{8}_{\rm A}}$ and $V_{\Xi\Lambda;\Xi\Sigma} = V_{\Xi\Sigma;\Xi\Lambda} =$

$\frac{1}{2}V^{\mathbf{10}} - \frac{1}{2}V^{\mathbf{8}_\mathrm{A}}$, which explains (i) existence of the weak attractive pocket in the central potentials of $\Xi\Lambda$-$\Xi\Lambda$ and $\Xi\Sigma$-$\Xi\Sigma$ at medium distance, (ii) similarity between the potentials of $\Xi\Lambda$-$\Xi\Lambda$ and $\Xi\Sigma$-$\Xi\Sigma$ both for central and tensor potentials, and (iii) weak tensor potentials of $\Xi\Lambda$-$\Xi\Sigma$ and $\Xi\Sigma$-$\Xi\Lambda$.

Due to the similar reason as before, we replace the factors $e^{(m_\Xi+m_\Lambda)t}$ and $e^{(m_\Xi+m_\Sigma)t}$ in Eq. (5.2) by products of two-point correlators of Ξ, Λ and Σ. We also replace the factors $\zeta^{\pm t/a}$ by the ratio of two-point correlators of Λ and Σ due to a technical reason. Therefore, although t-dependences of these potentials are mild, t should be large enough to achieve the ground state saturations of Ξ, Λ and Σ, i.e., $t \gtrsim 20$.

6. Summary

We have presented our results of the hyperon-hyperon potentials in $S=-3$ sector by using the 2+1 flavor QCD gauge configurations at almost the physical point ($m_\pi \simeq 146$ MeV) on the huge spatial volume $L \simeq 8.1$ fm generated on 96^4 lattice by K computer at AICS. To obtain the potentials, we have used non-relativistic approximations of the time-dependent Schrödinger-like equations. We have presented $\Xi\Sigma$ potentials for $I=3/2$ and $\Xi\Lambda$-$\Xi\Sigma$ coupled channel potentials for $I=1/2$. We have seen that qualitative behaviors are consistent with those in the flavor SU(3) limit.

Acknowledgments

We thank members of PACS Collaboration for the gauge configuration generation. Lattice QCD calculations have been performed on the K computer at RIKEN, AICS (Nos. hp120281, hp130023, hp140209 hp150223, hp150262, hp160211), HOKUSAI FX100 computer at RIKEN, Wako (G15023, G16030) and HA-PACS at University of Tsukuba (Nos.14a-20, 15a-30). We thank ILDG/JLDG [9] which serves as an essential infrastructure in this study. This work is supported in part by MEXT Grand-in-Aid for Scientific Research JP25400244, SPIRE (Strategic Program for Innovative REsearch) Field 5 project and "Priority Issue on Post-K computer" (Elucidation of the Fundamental Laws and Evolution of the Universe).

References

[1] N. Ishii, S. Aoki and T. Hatsuda, Phys. Rev. Lett. **99** (2007) 022001 [nucl-th/0611096].

[2] S. Aoki, T. Hatsuda and N. Ishii, Prog. Theor. Phys. **123** (2010) 89 [arXiv:0909.5585 [hep-lat]].

[3] S. Aoki *et al.* [HAL QCD Collaboration], Proc. Japan Acad. B **87** (2011) 509 [arXiv:1106.2281 [hep-lat]].

[4] S. Aoki *et al.* [HAL QCD Collaboration], PTEP **2012** (2012) 01A105 [arXiv:1206.5088 [hep-lat]].

[5] K.-I. Ishikawa *et al.* [PACS Collaboration], PoS LATTICE **2015** (2016) 075 [arXiv:1511.09222 [hep-lat]].

[6] N. Ishii *et al.* [HAL QCD Collaboration], Phys. Lett. B **712** (2012) 437 [arXiv:1203.3642 [hep-lat]].

[7] N. Ishii *et al.*, PoS LATTICE **2015** (2016) 087.

[8] T. Inoue *et al.* [HAL QCD Collaboration], Nucl. Phys. A **881** (2012) 28 [arXiv:1112.5926 [hep-lat]].

[9] http://www.lqcd.org/ildg/ and http://www.jldg.org/